Molecular Therapy
Methods & Clinical Development
Original Article

Central nervous system-targeted adeno-associated virus gene therapy in methylmalonic acidemia

Francis J. May,[1,2,3] PamelaSara E. Head,[1] Leah E. Venturoni,[1] Randy J. Chandler,[1] and Charles P. Venditti[1]

[1]Organic Acid Research Section, Medical Genomics and Metabolic Genetics Branch, National Human Genome Research Institute, National Institutes of Health (NIH), Bethesda, MD, USA; [2]NIH Medical Research Scholars Program, Bethesda, MD, USA; [3]Cleveland Clinic Lerner College of Medicine of Case Western Reserve University, Cleveland, OH, USA

Methylmalonic acidemia (MMA) is a severe metabolic disorder most commonly caused by a mutation in the methylmalonyl-CoA mutase (*MMUT*) gene. Patients with MMA experience multisystemic disease manifestations and remain at risk for neurological disease progression, even after liver transplantation. Therefore, delivery of MMUT to the central nervous system (CNS) may provide patients with neuroprotection and, perhaps, therapeutic benefits. To specifically target the brain, we developed a neurotropic PHP.eB vector that used a CaMKII neuro-specific promoter to restrict the expression of the *MMUT* transgene in the neuraxis and delivered the adeno-associated virus (AAV) to mice with MMA. The PHP.eB vector transduced cells in multiple brain regions, including the striatum, and enabled high levels of expression of MMUT in the basal ganglia. Following the CNS-specific correction of MMUT expression, disease-related metabolites methylmalonic acid and 2-methylcitrate were significantly ($p < 0.02$) decreased in serum of treated MMA mice. Our results show that targeting MMUT expression to the CNS using a neurotropic capsid can decrease the circulating metabolite load in MMA and further highlight the benefit of extrahepatic correction for disorders of organic acid metabolism.

INTRODUCTION

Methylmalonic acidemia (MMA) is a heterogenous genetic disorder most commonly caused by a mutation in the methylmalonyl-CoA mutase (*MMUT*) gene, which codes for the ubiquitously expressed mitochondrial enzyme methylmalonyl-CoA mutase.[1] MMUT, with its cofactor 5′deoxyadenosylcobalamin (a form of vitamin B12), plays a key role in catabolism of branched-chain amino acids, odd-chain fatty acids, propionate, and cholesterol. Loss of function of MMUT results in the accumulation of metabolic intermediates that cause a range of phenotypes, with the most severe subtype associated with a neonatal presentation of encephalopathy, metabolic acidosis, and death, if not promptly treated.[1] The recalcitrant nature of the recurrent metabolic instability experienced by patients, and the associated mortality and morbidity, has led to liver transplantation and, in parallel, the development of liver-targeted genomic therapies as possible alternatives to solid organ transplantation.[2–5]

Despite the efficacy of successful liver transplantation in the correction of the metabolic instability that characterizes MMA, some patients have experienced metabolic strokes in the basal ganglia after transplantation.[6] The stroke syndrome follows a typical course, with bilateral infarcts observed in the globus pallidus and striatum, highlighting the importance of these regions as a target for a gene therapy.[7,8] Therefore, for gene delivery of *MMUT* to be most effective, targeting of the central nervous system (CNS) may be required in addition to targeting of the liver.[8,9]

Some adeno-associated viruses (AAVs), such as AAV9, can penetrate the CNS after systemic delivery and widely transduce neurons, which has enabled the development of gene therapy for disorders previously considered untreatable, such as spinal muscular atrophy type 1.[10] However, improving the delivery of therapeutic transgenes to the CNS to achieve persistent expression remains a fundamental challenge for AAV gene therapy and for MMA in particular, given that extra-hepatic disease progression can occur after liver transplantation.[4,11] Systemic delivery of an AAV vector that can cross the blood-brain barrier and then transduce a wide variety of cell types in the CNS has several advantages over other injection routes such as intrathecal delivery, such as more widespread transduction of cells throughout the body as well as the neuroaxis. Most gene therapies for MMA target the liver, a key site of metabolism that most wild-type (WT) AAV capsids readily transduce at high levels.[5] By using a capsid and promoter that, in combination, can specifically transduce the CNS and not the liver, we hope to address whether there is a benefit of "full-body therapy" or therapy that includes non-hepatic tissues.

As a first step toward in the development of a vector to restore CNS expression of MMUT, we explored the cellular expression pattern of endogenous *Mmut* mRNA to understand the targets for transduction and tested a variety of AAV9 or PHP.eB reporter vectors for CNS

Received 8 November 2020; accepted 6 April 2021;
https://doi.org/10.1016/j.omtm.2021.04.005.

Correspondence: Charles P. Venditti, MD, PhD, Building 10, Room 7N248A, National Institutes of Health, Bethesda, MD 20892-4472, USA.
E-mail: venditti@mail.nih.gov

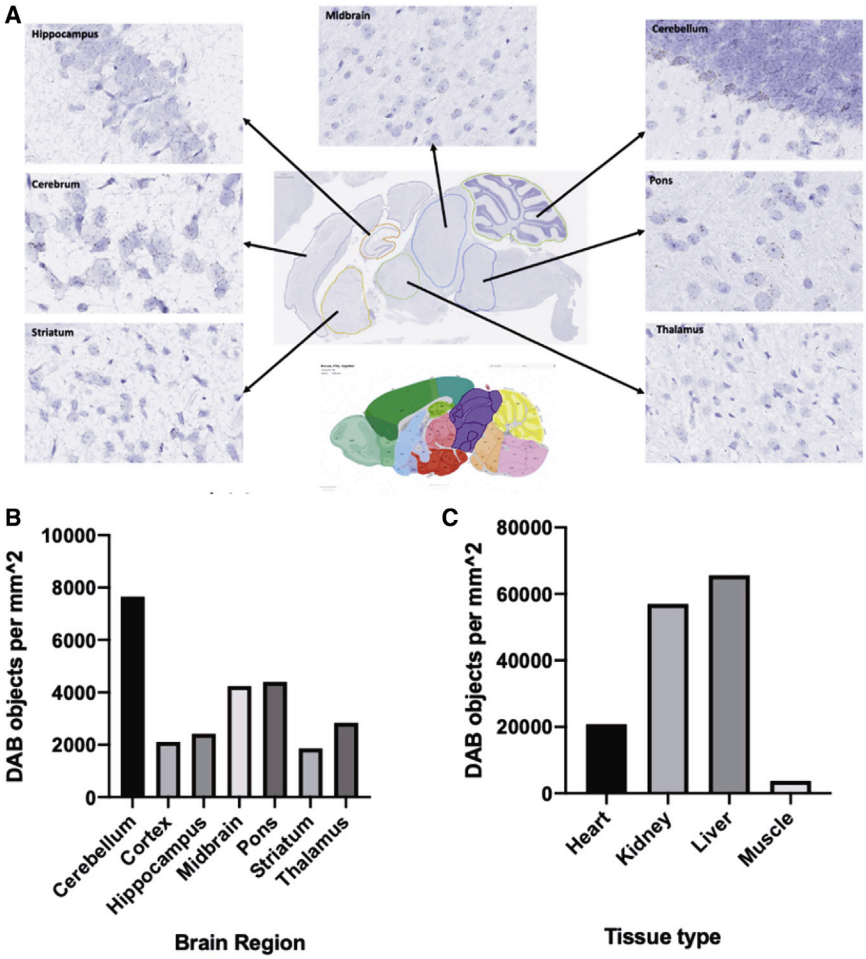

Figure 1. Native *Mmut* expression

(A) RNA in situ hybridization of native Mmut RNA in an untreated Mmut+/ mouse brain shown at 100 magnification. Shown by region in a sagittal section of mouse brain (A Hippocapmus; B Cerebrum; C Straitum; D Thalamus; E Cerebellum; F Pons; G Hippocapmus). Punctate, intracytoplasmic staining was observed distributed throughout all regions in cells morphologically consistent with neurons. (B) RNA in situ hybridization showed expression of native Mmut throughout the brain (n = 1). (C) Survey of non-CNS tissues showed native expression highest in the liver and kidneys (n = 1; refer to Figure S2 for images).

tropism in a mouse model of juvenile MMA.[12] Of note, *Mmut*$^{-/-}$;Tg$^{\text{INS-MCK-}Mmut}$ mice lack Mmut expression in the CNS but are viable by virtue of expression of a rescue transgene in the skeletal muscle and recapitulate the increased mortality, growth retardation, metabolic fragility, and hepatorenal pathology seen in patients with MMA. We then prepared a therapeutic PHP.eB vector to express *MMUT* under the control of the neuro-specific CaMKII promoter and delivered via the systemic circulation to *Mmut*$^{-/-}$;Tg$^{\text{INS-MCK-}Mmut}$ mice. Transgene expression in the brain was noted, specifically in the striatum and choroid plexus, two important targets for expression of MMUT, with an accompanying improvement in the levels of pathometabolites in the treated mutant mice. Our results support the suggestion that targeting both hepatic and extra-hepatic tissues, including the CNS, may be beneficial for the treatment of MMA, a disease which displays conditional cell autonomous pathophysiology.[13]

RESULTS

Endogenous Mmut expression and reporter transduction and expression in the CNS

The native *Mmut* expression in tissues of WT mouse was first surveyed to identify relative expression throughout various tissue and cell types. We collected brain, liver, kidney, heart, and skeletal muscle from an untreated phenotypically WT heterozygous *Mmut*$^{+/-}$ mouse at weaning. RNA *in situ* hybridization showed expression of native *Mmut* (Figures 1 and 5) in all brain regions investigated, including the striatum, choroid plexus, hippocampus, midbrain, pons, thalamus, and cerebral cortex. The staining was observed to be intracellular, with diffuse cytosolic punctation. A survey of non-CNS tissues showed native *Mmut* expression highest in the kidneys and liver, with lower levels present in the skeletal muscle and cardiac muscle, consistent with Mmut protein assays from previous studies (Figure 1C and S2).[14]

We then used AAV reporter vectors to investigate CNS transduction and to guide design of a therapeutic vector. Neonatal *Mmut*$^{-/-}$;Tg$^{\text{INS-MCK-}Mmut}$ mice and *Mmut*$^{+/-}$ littermates were injected with EGFP reporter AAV vectors (Table 1) on day-of-life (DOL) 0 via the retro-orbital sinus at a dose of 1e11 GC (genome copies)/pup, and tissue was collected on day 21. AAV transduction was quantified by EGFP expression in select brain regions, including the cerebrum, cerebellum, striatum, choroid plexus, hippocampus, thalamus, hypothalamus, and pons (Figure 2). Expression of EGFP after treatment with reporter vectors was variable between PHP.eB and AAV9 serotypes (Figure 3), and comparison of EGFP expression across brain regions revealed global transduction that was most pronounced in the choroid plexus ($p = 0.0071$, $n = 3$) (Figure 3F). Brain tissue from a separate cohort of mice, treated in an identical fashion, was co-stained for green fluorescent protein (GFP) and the neuronal marker NeuN. The PHP.eB and AAV9 vectors also directed transgene expression of GFP in the striatum, in cells that co-stained with the neuronal marker NeuN (Figure 3D). In the cerebellum and choroid plexus, numerous overlapping NeuN+ cells skewed analyses based on the percent of NeuN+ cells that were also GFP+ and therefore were excluded from direct comparison with other regions (Figures 3G and S1). In regions where cell architecture is such that many neurons appear to overlap in the visual field, such as the hippocampus

Table 1. AAV vectors

Vector name	Capsid	Promoter	Transgene	Other
AAV9-CBA-GFP	AAV9	*CBA*	*GFP*	*CMV, WPRE*
AAV9-CaMKII-GFP	AAV9	*CaMKII*	*GFP*	NA
PHP.eB-CBA-GFP	PHP.eB	*CBA*	*GFP*	*CMV*
PHP.eB-CaMKII-GFP	PHP.eB	*CaMKII*	*GFP*	NA
PHP.eB-CaMKII-MMUT	PHP.eB	*CaMKII*	*MMUT*	NA

Listed as capsid-promoter-transgene. PHP.eB-CaMKII-MMUT is the therapeutic vector; all others are reporter vectors carrying a GFP transgene. CaMKII, Ca^{2+}/calmodulin-dependent protein kinase; CBA, chicken beta-actin; GFP, green fluorescent protein; WPRE, woodchuck hepatitis virus posttranscriptional regulatory element; CMV, cytomegalovirus enhancer; NA, not applicable.

and cerebellum, NeuN+ cells appear to stain a brighter red color. There was no significant effect of genotype on distribution of GFP+/NeuN+ cells ($p = 0.8441$, *Mmut*$^{-/-}$;Tg$^{\text{INS-MCK-}Mmut}$ mice versus *Mmut*$^{+/-}$ controls).

AAV delivery of MMUT transgene in a murine model of MMA: biodistribution, expression, and metabolic effects

Based on favorable CNS transduction by the CaMKII-GFP vectors and alignment with endogenous *Mmut* expression, a PHP.eB-CaMKII-MMUT vector (Table 1) was prepared and used to treat *Mmut*$^{-/-}$;Tg$^{\text{INS-MCK-}Mmut}$ mice or *Mmut*$^{+/-}$ littermates at DOL 0 using the same dose and route as reporter vectors (retro-orbital injection of 1e11 GC/pup).

In *Mmut*$^{-/-}$;Tg$^{\text{INS-MCK-}Mmut}$ mice that were treated with PHP.eB-CaMKII-MMUT, exploratory RNA *in situ* hybridization studies demonstrated exogenous AAV-delivered *MMUT* expression in all brain regions assessed (Figure 4). Choroid plexus studies were limited because only a single stained slide section from each cohort retained adequate tissue from this region for analysis (Figure 5). *MMUT* expression appeared most pronounced in the ventral regions of the brain, including the ventral striatum and hypothalamus (Figures 4 and 6). No *MMUT* RNA expression was detected in PHP.eB-CaMKII-MMUT-treated liver tissue (Figures 6 and S2). The viral genome copy number of mice treated with PHP.eB-CaMKII-MMUT (Figure 6) was observed by ddPCR digital droplet PCR in both liver and brain tissue. The genome copy number in the brain and liver was variable but not statistically different between tissues or genotypes ($p = 0.7262$, $n = 4$ each group).

At the cellular level, *MMUT* RNA staining in the brain of PHP.eB-CaMKII-MMUT-treated *Mmut*$^{-/-}$;Tg$^{\text{INS-MCK-}Mmut}$ mice was intracytoplasmic, punctate, and appeared in a similar regional distribution as the endogenous *Mmut* in *Mmut*$^{+/-}$ mice. Some of the AAV-transduced cell staining appeared as aggregates. Cells were morphologically consistent with neurons (Figures 4 and 5). We used the H-score semiquantitative scoring method for stain measurement instead of DAB 3,3′-Diaminobenzidine staining, which counts individual points and therefore would inaccurately assess aggregate staining.

Mmut$^{-/-}$;Tg$^{\text{INS-MCK-}Mmut}$ mice had significantly lower body mass compared to phenotypically WT *Mmut*$^{+/-}$ littermates (Figure S2), as reported in previous studies with this transgenic mouse model.[15] Total body mass in PHP.eB-CaMKII-MMUT-treated *Mmut*$^{-/-}$;Tg$^{\text{INS-MCK-}Mmut}$ mice was not significantly different compared to MMA GFP reporter controls.

Plasma concentrations of disease-related metabolites, methylmalonic acid and total 2-methylcitrate (MC), were measured in both *Mmut*$^{-/-}$;Tg$^{\text{INS-MCK-}Mmut}$ mice and *Mmut*$^{+/-}$ littermates after therapeutic or reporter AAV treatment on DOL 21, when a necropsy was performed. Compared to untreated *Mmut*$^{-/-}$;Tg$^{\text{INS-MCK-}Mmut}$ mice, PHP.eB-CaMKII-MMUT-treated mutant mice had significant decreases in methylmalonic acid and MC but did not achieve normal levels. The plasma levels of 2-methylcitrate isoform II (MCII) were significantly decreased in MMUT-treated *Mmut*$^{-/-}$;Tg$^{\text{INS-MCK-}Mmut}$ mice compared to controls, while 2-methylcitrate isoform I (MCI) was not. Interestingly, the ratio of MCI to MCII was decreased in MMUT-treated *Mmut*$^{-/-}$;Tg$^{\text{INS-MCK-}Mmut}$ mice compared to those who were treated with a GFP reporter (Figures 7 and S3). Whole-brain tissue was mechanically homogenized, and levels of metabolites were measured in the same manner. *Mmut*$^{-/-}$;Tg$^{\text{INS-MCK-}Mmut}$ mice had significantly higher levels of both methylmalonic acid and 2-MC compared to *Mmut*$^{+/-}$ littermates regardless of treatment group. Unlike the systemic metabolite levels, in the brain homogenate metabolite measurements there was no significant decrease in methylmalonic acid or 2-MC seen when comparing MMUT-treated to GFP-reporter-treated MMA mice. No difference in the ratio of MCI/MCII was observed when comparing across genotype and treatment group.

In this same cohort of mice, MMUT protein expression in brain deep gray matter and liver was surveyed. Immunoblotting demonstrated ample MMUT protein in the brains, but not the livers, of *Mmut*$^{-/-}$;Tg$^{\text{INS-MCK-}Mmut}$ mice treated with PHP.eB-CaMKII-MMUT, which was expected because the vector contains the neuro-specific CaMKII promoter. No MMUT protein expression was seen in reporter GFP-treated *Mmut*$^{-/-}$;Tg$^{\text{INS-MCK-}Mmut}$ mice because these animals do not express endogenous Mmut protein in the brain or liver. In reporter GFP-treated *Mmut*$^{+/-}$ littermates, endogenous Mmut was readily detected by western blot in both brain and liver (Figure 9).

DISCUSSION

Disease-related manifestations related to MMA, such as metabolic stroke of the basal ganglia, have been reported in patients even after successful liver transplant, leading us to hypothesize that in addition to treatment directed at the liver, patients may derive additional benefit from gene delivery to extra-hepatic tissues such as the CNS. We therefore designed an AAV gene therapy vector using a neurotropic capsid, PHP.eB, and a neuro-specific promoter, CaMKII, to direct CNS-specific expression of MMUT.

We first explored the expression of native *Mmut* using RNA *in situ* hybridization in a mouse with WT *Mmut* (Figure 1). *Mmut* RNA expression appeared to be highest in liver, kidney, and heart. Skeletal

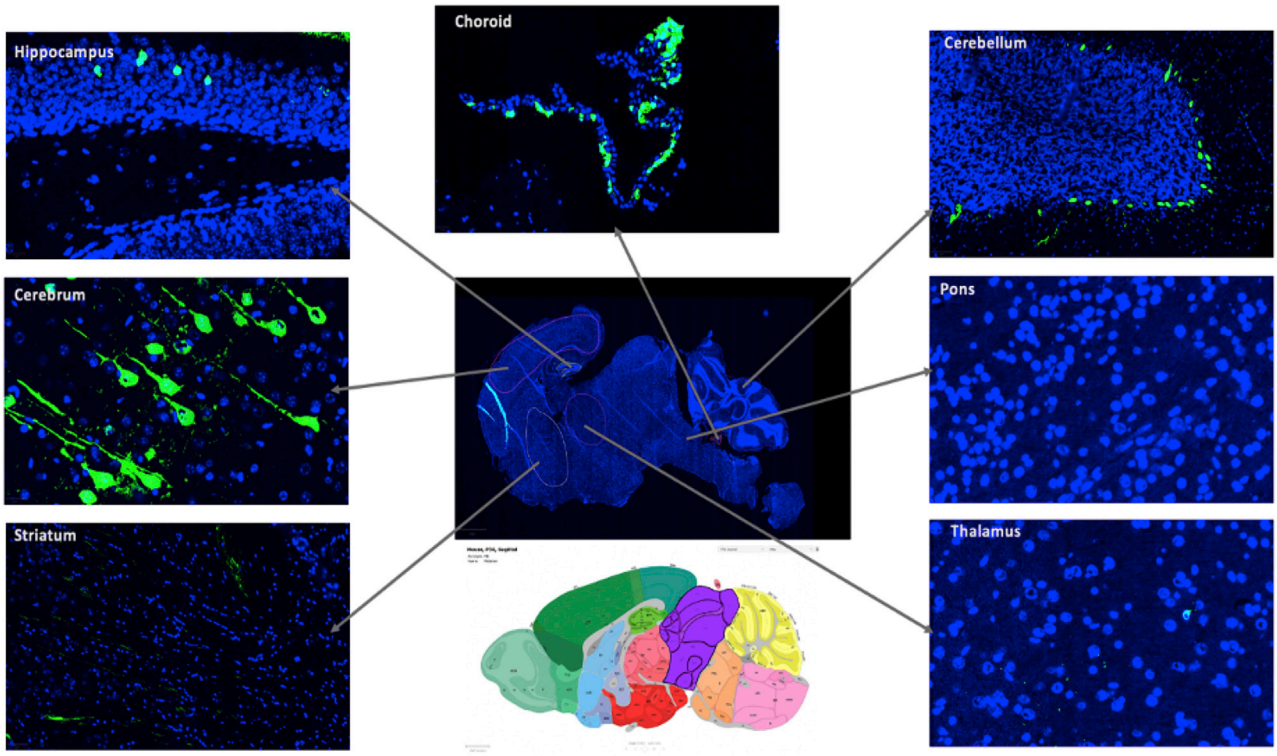

Figure 2. GFP fluorescence in the *Mmut*$^{-/-}$;Tg$^{INS\text{-}MCK\text{-}Mmut}$ mouse brain

Mice were treated DOL 0 with retro-orbital injection of PHP.eB-CBA-GFP at 1e11 GC/mouse, and tissue was collected DOL 21. Cells in the hippocampus, cerebrum, cerebellum, and comprising the choroid plexus display strong signal shown at 100× magnification.

muscle and brain had comparable levels of expression, and all brain regions assessed had native *Mmut* expression (Figure 1B). These RNA *in situ* hybridization studies are consistent with the known expression patterns of methylmalonyl-CoA mutase and its mRNA in mice and humans.[16–18] In the rat brain, methylmalonyl-CoA mutase expression may be restricted to neuronal cells and may be increased in the CNS early in neurodevelopment to levels even higher than expression levels in liver.[19] Therefore, if MMUT expression is likewise mainly in neuronal cells in humans and increased in early development, neuro-targeted MMUT correction in the neonatal period may be especially critical in MMA.

To assess the ability of a therapeutic vector to target brain regions with known *Mmut* expression, we performed reporter studies with vectors combining CNS-tropic AAV capsids with a promoter that restricts expression to the CNS. For AAV capsids, we chose to use AAV9 and PHP.eB. AAV9 is a capsid with strong tropism to the CNS, among other tissues, that has been extensively studied and is already US Food and Drug Administration (FDA) approved for treatment of spinal muscular atrophy.[20] PHP.eB is an engineered AAV capsid related to PHP.B that has shown remarkable propensity to transduce the CNS of certain mouse strains when administered systemically, more efficiently than any known WT AAV, including AAV9.[21,22] The CaMKII promoter is a well-characterized neuro-specific promoter, which has been used in an AAV9 vector that improved the lifespan of mice with Niemann-Pick disease, type C1.[10] Other neurotropic promoters such as the synapsin promoter and methyl-CpG-binding protein-2 (MeCP2) promoter were also considered, but CaMKII was chosen due to its relatively higher levels of neuraxis expression and proven efficacy in a severe neurodegenerative mouse model.[23,24] The chicken beta-actin (CBA) promoter, commonly used in AAV proof-of-concept vectors, drives ubiquitous gene expression and was selected as a comparator.[24,25] Immunohistochemistry of EGFP expression from reporter vectors demonstrated variable performance between capsid serotypes, with relatively high transduction of the choroid plexus (Figures 2 and 3). As a key site of small-molecule transport and metabolism between the brain parenchyma and the cerebrospinal fluid (CSF), targeting the choroid plexus could, in theory, assist in reduction of toxic metabolite accumulation in the CNS, which is thought to contribute to neurological disease in MMA. Of note, the tropism demonstrated by reporter vectors showed no statistically significant difference in transduction between *Mmut*$^{-/-}$; Tg$^{INS\text{-}MCK\text{-}Mmut}$ mice and *Mmut*$^{+/-}$ littermates (Figure 3).

Based on the successful transduction of the CNS using reporter AAV vectors, a therapeutic vector was created using a PHP.eB capsid with the neuro-specific CaMKII promoter driving expression of MMUT. The neuro-specificity of the promoter was designed to allow us to

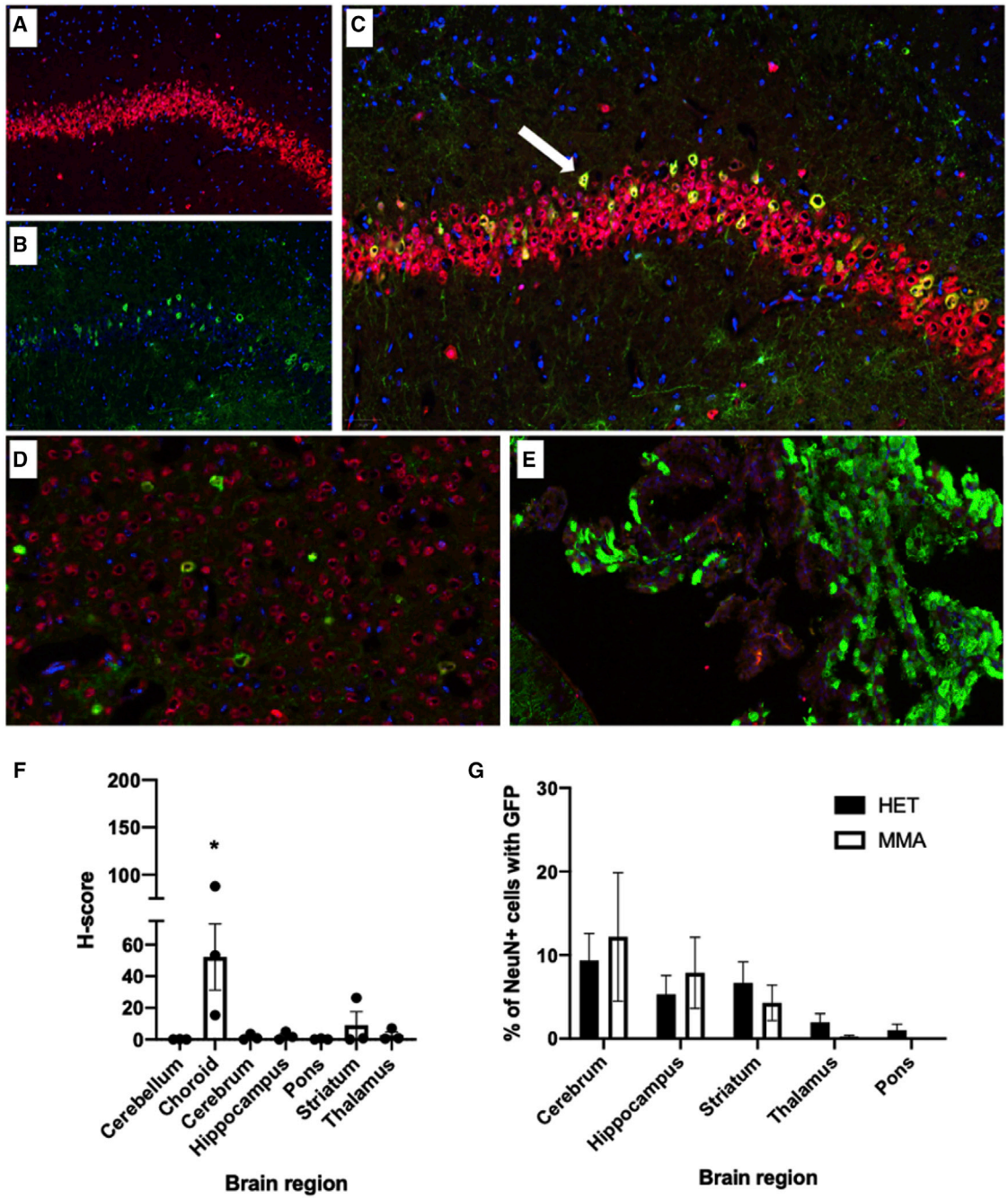

Figure 3. EGFP-reporter-treated mice

Hippocampus of a *Mmut*$^{+/-}$ mouse treated on DOL 1 with AAV9-CBA-GFP at 100× magnification (A–C). Cells are stained with nuclear DAPI+ stain in blue (all images), NeuN+ stain in red (A), GFP+ stain in green (B), and all three stains overlaid appear yellow-green (white arrow) (C). Following retro-orbital injection of PHP.eB-CBA-GFP of mice on DOL 0, the striatum (D) and choroid plexus (E) of an *Mmut*$^{-/-}$;Tg$^{\text{INS-MCK-}Mmut}$ mice, labeled MMA, at 200× magnification show strong GFP fluorescence in neuronal cells. (F) H-score of GFP positivity in MMA mice treated with PHP.eB-CBA-GFP reporter vector ($p = 0.0071$, $n = 3$). (G) Percent co-positivity of NeuN and GFP by brain region in *Mmut*$^{+/-}$ mice, labeled HET, or *Mmut*$^{-/-}$;Tg$^{\text{INS-MCK-}Mmut}$ mice treated with PHP.eB-CaMKII-GFP. No significant difference was found for any region when stratified by genotype ($p = 0.8441$, *Mmut*$^{-/-}$;Tg$^{\text{INS-MCK-}Mmut}$ mice [$n = 4$] versus *Mmut*$^{+/-}$ controls [$n = 4$]).

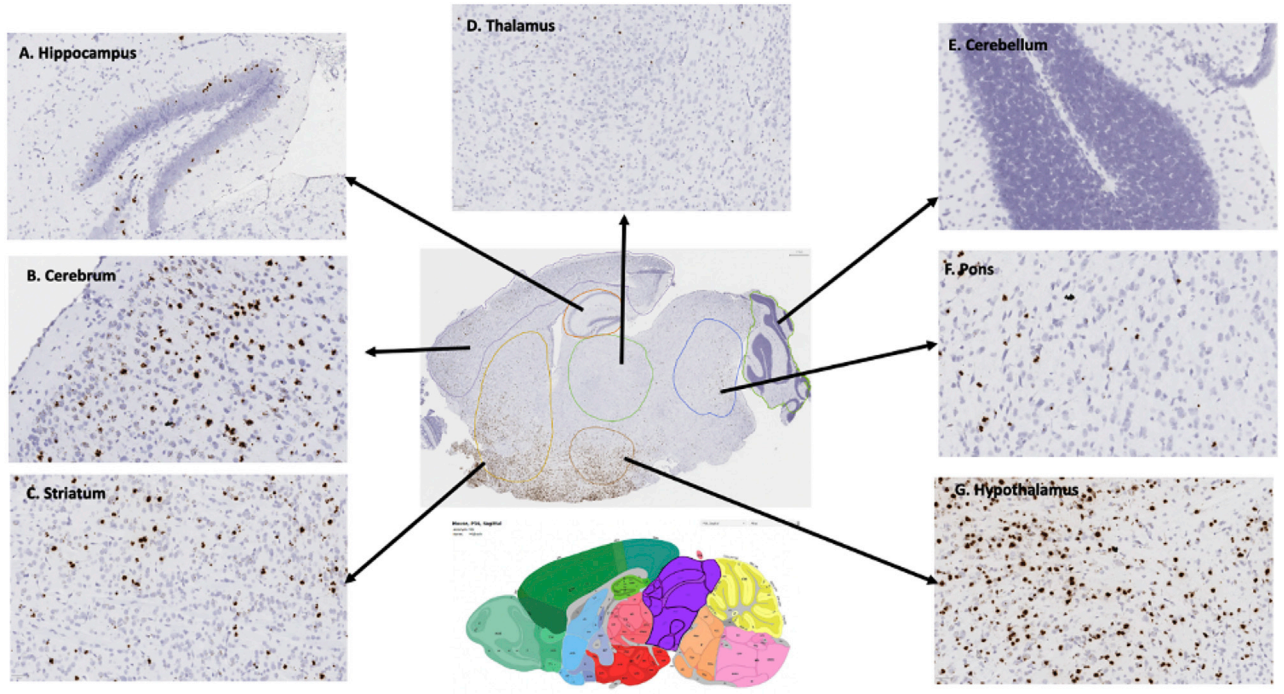

Figure 4. RNA *in situ* hybridization in the brain of *Mmut*$^{-/-}$;Tg$^{INS\text{-}MCK\text{-}Mmut}$ mice treated with PHP.eB-CaMKII-MMUT

Probe targeting *MMUT* RNA was quantified by region in a sagittal section of mouse brain, shown at 100× magnification. Mice were treated DOL 0 with retro-orbital injection of PHP.eB-CaMKII-MMUT at a dose of 1e11 GC/mouse, and tissue was collected DOL 21. Large aggregate staining was observed most commonly along with punctate; cytosolic staining was observed.

investigate the effect of isolated CNS delivery of the *MMUT* transgene in a murine MMA model. In *Mmut*$^{-/-}$;Tg$^{INS\text{-}MCK\text{-}Mmut}$ mice that were treated with PHP.eB-CaMKII-MMUT, ddPCR showed that viral genome copies were present in liver and brain tissue of both control and mutant mice (Figure 6). RNA *in situ* hybridization studies demonstrated *MMUT* expression in all regions of the brain assessed (Figures 4 and 6). As the site of highest expression of endogenous *Mmut* and a major site of AAV transduction, any off-target *MMUT* expression would be expected to be observed in liver tissue; however, no *MMUT* expression was observed by RNA *in situ* hybridization or

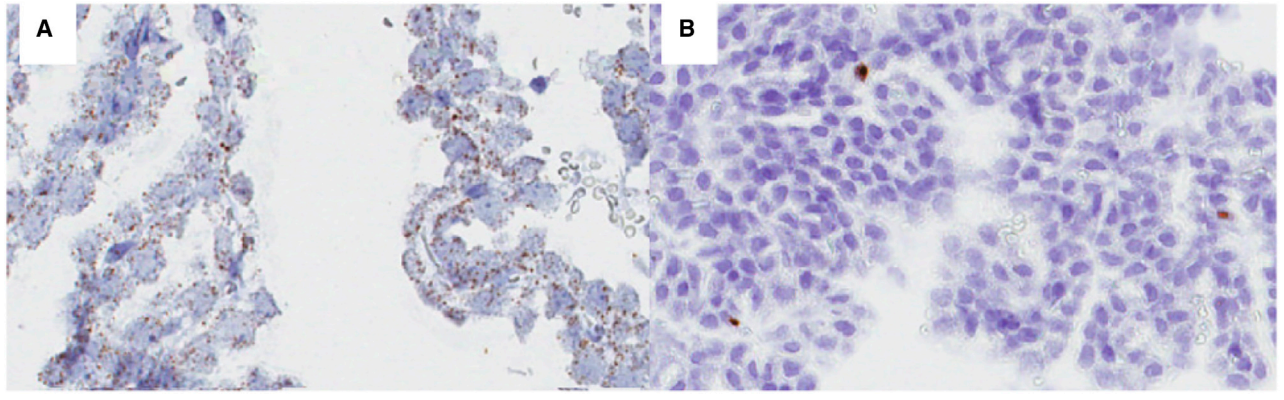

Figure 5. Native *Mmut* RNA expression compared to delivered *MMUT* in the choroid plexus

Native *Mmut* had high levels of diffuse, punctate expression in the choroid plexus of untreated *Mmut*$^{+/-}$ age-matched control mice (A) shown by *Mmut* RNA *in situ* hybridization at 200× magnification. Untreated *Mmut*$^{-/-}$;Tg$^{INS\text{-}MCK\text{-}Mmut}$ mice show no native *Mmut* expression (not shown). Following treatment with PHP.eB-CaMKII-MMUT at birth, *Mmut*$^{-/-}$;Tg$^{INS\text{-}MCK\text{-}Mmut}$ mice show limited expression of *MMUT* in the choroid plexus (B). The brown staining represents *MMUT* transgene expression. Choroid plexus tissue from a single mouse was adequately retained on prepared slides.

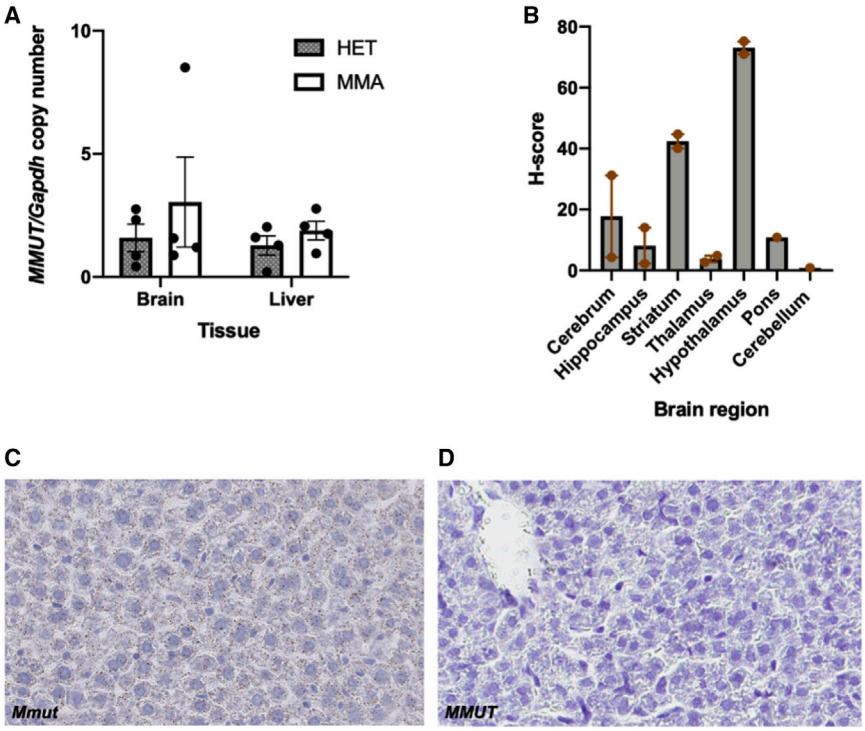

Figure 6. Biodistribution and expression

(A) Viral genome copy number. Ratio of copy number of *MMUT*/*Gapdh* DNA in *Mmut*$^{+/-}$, labeled HET, or *Mmut*$^{-/-}$;Tg$^{INS\text{-}MCK\text{-}Mmut}$ mice, labeled MMA, were treated with 1e11 GC/mouse of PHP.eB-CaMKII-MMUT therapeutic vector on DOL 1 (n = 4 each group). Whole-brain and liver tissue were collected on DOL 21. Average number of genome copies per cell was determined from ddPCR of tissue homogenate by normalizing amplified counts for a probe specific for *MMUT*, present in viral genomic episomes, to counts of *Gapdh*. (B) RNA *in situ* hybridization. H-score quantification of *MMUT* mRNA stained using RNA *in situ* hybridization in brain tissue of PHP.eB-CaMKII-MMUT-treated *Mmut*$^{-/-}$;Tg$^{INS\text{-}MCK\text{-}Mmut}$ mice collected DOL 21 (n = 2). (C) *Mmut* expression in untreated liver. Endogenous *Mmut* mRNA is highly expressed in liver tissue, shown here at 100× magnification following staining of *Mmut* by RNA *in situ* hybridization in an untreated *Mmut*$^{+/-}$ mouse. (D) *MMUT* expression in treated liver. No *MMUT* mRNA staining was present in liver tissue of PHP.eB-CaMKII-MMUT-treated *Mmut*$^{-/-}$;Tg$^{INS\text{-}MCK\text{-}Mmut}$ mice.

by western blotting studies (Figures 6 and 7). Adequate choroid plexus tissue for analysis was only retained on stained slides for one mouse from each cohort and demonstrated high levels of endogenous *Mmut* expression and successful transduction of exogenous *MMUT* when visualized (Figure 5). There was pronounced *MMUT* transgene expression in the ventral regions of the brain, including the ventral striatum and hypothalamus (Figures 4 and 6). The staining patterns included both punctate and aggregate staining in some regions. The observed variability in staining between regions, seen even within a single brain, was not seen in positive control slides, so it is more likely to reflect true variability in *MMUT* expression rather than being attributed as an artifact of the stain. In the PHP.eB-CaMKII-MMUT-treated *Mmut*$^{-/-}$;Tg$^{INS\text{-}MCK\text{-}Mmut}$ mice, western blot of deep gray matter brain tissue demonstrated presence of MMUT, which was readily detected but present at lower levels than native MMUT expression in *Mmut*$^{+/-}$ mice (Figure 7). No off-target expression of MMUT by the CaMKII promoter was detected in the livers of treated MMA mice, and, further, no Mmut protein expression was detected in the livers of untreated *Mmut*$^{-/-}$;Tg$^{INS\text{-}MCK\text{-}Mmut}$ mice (Figure 6). These results are consistent with restriction of MMUT expression by CaMKII promoter to the CNS and further demonstrate that systemic AAV vector delivery can efficiently transduce the basal ganglia, resulting in MMUT expression in a region of the brain susceptible to metabolic strokes in MMA.

Mmut$^{-/-}$;Tg$^{INS\text{-}MCK\text{-}Mmut}$ mice treated with the therapeutic PHP.eB-CaMKII-MMUT vector also had reduced levels of the serum pathometabolites, methylmalonic acid and MC, when compared to age-matched *Mmut*$^{+/-}$ littermates 3 weeks post-treatment (Figure 8) The relative reduction of these metabolite levels in the systemic circulation was surprising, given that in our study therapeutic MMUT expression was limited to the CNS. Methylmalonic acid and MC are known to be elevated in both CSF and serum of patients with MMA.[1,26,27] In an earlier study characterizing *Mmut* knockout mice, MC was found to be elevated in the affected mice in all fluids and tissues examined.[15] Additionally, the levels of both metabolites tend to be more elevated in the CSF (brain tissue) than plasma.[27] The ratio of the stereoisomer MCI to MCII was shown to increase more in the brain compared to the periphery as the illness progressed in the *Mmut* knockout mice, although this phenomenon has not been well studied.[15,26,27] While the nature of exchange of the metabolites, MC and methylmalonic acid, between the CSF and blood is not fully understood, one hypothesis proposes that metabolites produced in the CNS become trapped in CNS parenchyma and/or CSF due to a limitation of dicarboxylic acid transport at the blood-brain barrier.[28–31] In our studies, the ratio of MCI/MCII was decreased in the periphery of the treated MMA mice, consistent with the effects of CNS correction. We measured disease-related metabolite levels in whole-brain tissue homogenate but did not see the same reduction we observed in serum levels (Figures 8 and 9). It is possible that despite corrected CNS expression of MMUT, blood-brain barrier transport has a larger overall effect on distribution of metabolites, so that intraparenchymal elevation of metabolites persists while systemically a decrease is observed. Additional studies, including measurements of CSF levels of methylmalonic acid and MCI and II in treated versus untreated MMA mice, will be needed to help elucidate the nature of the biochemical correction and provide insight into the mechanism of exchange of these toxic metabolites between the CSF and the periphery. The choroid plexus may also contribute to the

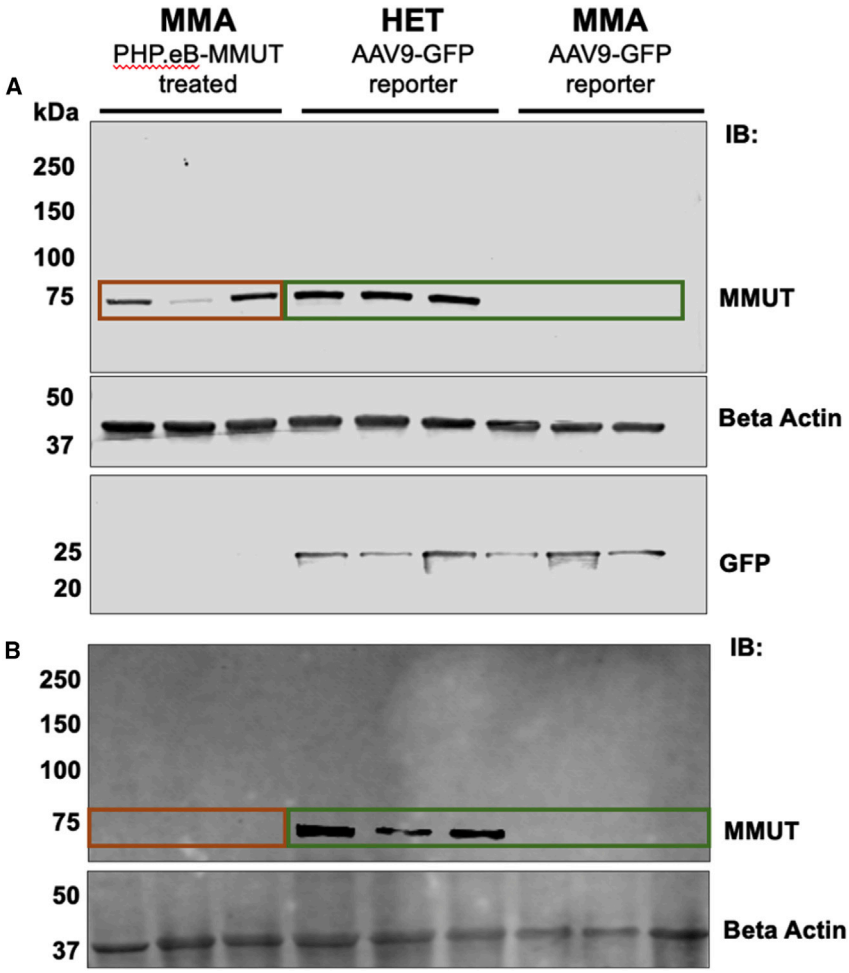

Figure 7. Brain and liver MMUT expression after treatment with AAV PHP.eB-CaMKII-MMUT or a GFP reporter

(A) Deep gray matter brain tissue collected at DOL 21 following treatment with therapeutic or reporter vectors on DOL 1. The cortex and cerebellum were removed from each brain and 50 μg of lysate from the remaining tissue was loaded into each well. Western blotting using anti-MMUT antibody reveals a band of ~75 kDa that is present in the brain extracts of the *Mmut*$^{+/-}$ (labeled HET) AAV9-CBA-GFP-treated controls and in the PHP.eB-CaMKII-MMUT-treated *Mmut*$^{-/-}$;Tg$^{INS\text{-}MCK\text{-}Mmut}$ mice (labeled MMA) but is completely absent from the *Mmut*$^{-/-}$;Tg$^{INS\text{-}MCK\text{-}Mmut}$ GFP-treated controls. Blotting using anti-GFP antibody reveals a band at ~25 kDa present in the GFP-treated *Mmut*$^{-/-}$;Tg$^{INS\text{-}MCK\text{-}Mmut}$ and *Mmut*$^{+/-}$ control mice but absent in the PHP.eB-CaMKII-MMUT-treated *Mmut*$^{-/-}$;Tg$^{INS\text{-}MCK\text{-}Mmut}$ mice. (B) Liver tissue collected from same mice. Western blotting using anti-MMUT antibody reveals a band of ~75 kDa that is present in the liver extracts only of the *Mmut*$^{+/-}$ (labeled HET) and no band in the PHP.eB-CaMKII-MMUT-treated *Mmut*$^{-/-}$;Tg$^{INS\text{-}MCK\text{-}Mmut}$ mice or the *Mmut*$^{-/-}$;Tg$^{INS\text{-}MCK\text{-}Mmut}$ GFP-treated controls.

metabolism of MMA and MC, which seems likely given the transduction we have observed with the AAV vectors studied and the high levels of endogenous *Mmut* noted in WT mice by RNA *in situ* hybridization.

The clinical translation of our results with a PHP.eB vector will be limited, because this capsid's neurotropic properties depend on LY6A, a protein not found in non-human primates or humans.[32,33] Despite this caveat, PHP.B and related capsids continue to act as benchmarks for pre-clinical AAV gene therapy studies that target the CNS. In fact, in an exciting recent development, newly engineered, non-LY6A PHP-class capsids that retain efficiency for CNS transduction have been identified.[11,22] Therefore, we view the PHP.eB vector developed here as a proxy for what will be achieved with the next generation of neurotropic capsids, which hold great promise to enable CNS-targeted AAV gene therapy. Previous murine studies in our lab have used AAV9 as a CNS-targeted vector for treatment of the disease NPC1 and MMA, with demonstrated benefit.[10] Although AAV9 has been shown to have lower efficiency in CNS transduction compared to PHP.eB, AAV9 also has tropism to liver, making it an interesting option for a clinical scenario in which both liver and CNS transduction are desired, as we argue could be the case in MMA patients.[11]

Since the mouse model of MMA we used does not exhibit any obvious neurological phenotype, determining the effect of gene delivery on behavior, locomotion, or CNS symptoms was not possible. Given the cell-autonomous nature of MMA, we hypothesize that restoring MMUT expression in a regioselective fashion, specifically to brain regions impacted by the disease such as the striatum, could have a therapeutic and protective benefit. Additionally, the systemic reduction of toxic disease-related metabolites after CNS-directed gene therapy could potentially reduce the overall circulating metabolite load, and we speculate that targeting MMUT expression to the choroid plexus might provide additional systemic benefits, as has been noted in other mouse models.[34]

In aggregate, our experiments demonstrate that a CNS-tropic AAV vector can restore expression of MMUT in the CNS after systemic delivery in a mouse model of severe MMA. Using the CaMKII neuro-specific promoter, restoration of MMUT expression was limited to the CNS, notably those regions of the brain that are thought to be involved in disease progression such as the striatum, and metabolism at the blood-brain barrier, in the choroid plexus. The surprising reduction in systemic levels of toxic metabolites, with MMUT expression limited only to the CNS, supports the proposition that AAV-mediated CNS gene therapy will likely benefit patients with MMA and, further, could confer neuroprotection, even to those who have received liver transplantation.

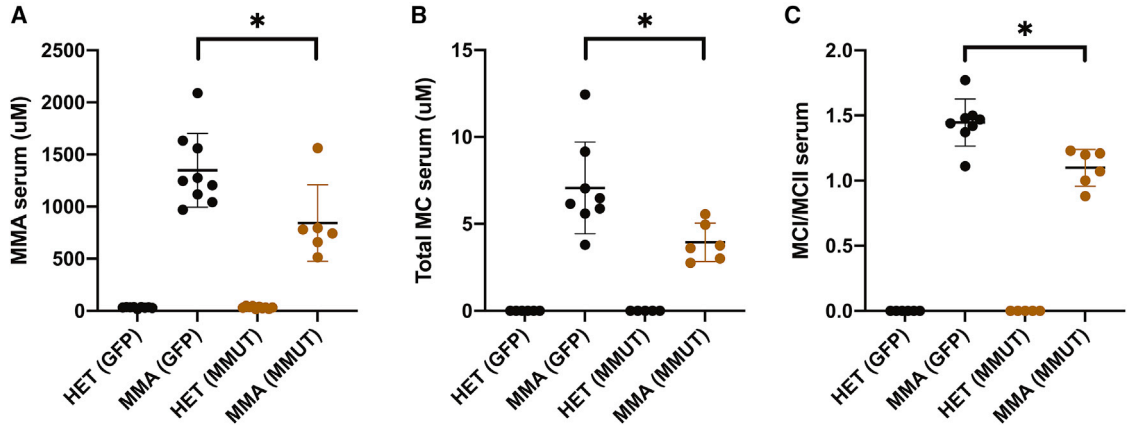

Figure 8. Effect of gene therapy on serum metabolites

Methylmalonic acid and 2-methylcitrate (MC) shown stratified by group in *Mmut*$^{+/-}$ (labeled HET), or *Mmut*$^{-/-}$;Tg$^{INS\text{-}MCK\text{-}Mmut}$ mice (labeled MMA), injected with a reporter (GFP, control vector) or treatment PHP.eB-CaMKII-MMUT vector (labeled MMUT). (A) Methylmalonic acid was significantly lower in *Mmut*$^{-/-}$;Tg$^{INS\text{-}MCK\text{-}Mmut}$ mice that were treated with PHP.eB-CaMKII-MMUT (n = 6) compared to *Mmut*$^{+/-}$ controls (n = 9, $p < 0.02$). (B) Total MC was significantly lower in *Mmut*$^{-/-}$;Tg$^{INS\text{-}MCK\text{-}Mmut}$ mice (labeled MMA) that were treated with PHP.eB-CaMKII-MMUT (n = 6, $p = 0.02$) compared to reporter control (n = 9). (C) In MMUT-treated *Mmut*$^{-/-}$;Tg$^{INS\text{-}MCK\text{-}Mmut}$ mice (labeled MMA), the ratio MCI/MCII ($p < 0.0001$) was significantly decreased compared to those treated with a GFP reporter.

MATERIALS AND METHODS

Plasmid construction and AAV vector production

Therapeutic plasmids were cloned from a backbone of the expression vector pENN.AAV.CamKII0.4.eGFP.rBG (PL-C-PV1474), which was obtained from the University of Pennsylvania Vector Core. This vector contains transcriptional control elements from the mouse Ca^{2+}/calmodulin-dependent protein kinase II (CaMKII) promoter, cloning sites for the insertion of a complementary DNA, and the rabbit β-globin polyA signal, which were produced as previously described.[35] The GFP was replaced with a codon-optimized version of *MMUT*. Additional reporter plasmids expressing EGFP from a CaMKII or CBA promoter and cloned between WT AAV2 ITRs and pseudoserotyped in PHP.eB or AAV9 capsids were purchased (37825-PHP.eB, 37825-AAV9, 105541-AAV9) (Addgene, Watertown, MA, USA). Our reporter vectors were constructed with AAV9 or PHP.eB capsids, known to have CNS tropism.[10,11] Therapeutic *MMUT* plasmids were pseudoserotyped with PHP.eB capsids, purified by CsCl gradient centrifugation, aliquoted, titered, frozen, and then freshly diluted with PBS (Vigene Biosciences, Rockville, MD, USA).

Mouse model

Animal work was performed in accordance with the guidelines for animal care at NIH and the Guide for the Care and Use of Laboratory Animals (https://wol-prod-cdn.literatumonline.com/pb-assets/hub-assets/aasldpubs/Hepatology_1527-3350/guide-for-the-care-and-use-of-laboratory-animals-1542041308777.pdf). A knockout transgenic mouse model of MMA, with murine muscle creatine kinase (MCK) promoter to drive *Mmut* expression in the skeletal and cardiac muscle of the *Mmut*$^{-/-}$ mice, was used in our studies.[15] The background strains are enriched C57/BL6 and FVBN, which are largely permissive to PHP.B and PHP.eB capsid transduction of the CNS.[21,22] The resulting *Mmut*$^{-/-}$;Tg$^{INS\text{-}MCK\text{-}Mmut}$ animals, referred to as MMA mice in some figures, were rescued from the neonatal lethality observed in *Mmut*$^{-/-}$ mice but manifested the clinical and biochemical features of MMA, including severe growth retardation, fragility, massively elevated serum methylmalonic acid concentrations, and hepatorenal mitochondrial pathology.[3,15] Treated mice received AAV via retro-orbital injection 12–24 h postpartum. Mice were bled via retro-orbital sinus plexus sampling using a sterile glass capillary tube and weighed monthly. Controls were cohoused mice from the same litter. All mice were housed in microisolator cages on positive-pressure ventilated racks (Lab Products, Seaford, DE, USA), and cages were bedded with steam-sterilized hardwood bedding (Nepco Beta-Chips). Standard environmental enrichment for all mouse cages containing two or more animals was a pulped virgin cotton Nestlet (Ancare, Bellmore, NY, USA). Environmental enrichment for cages containing singly housed animals consisted of a Nestlet and a paper nesting product (Bed-R-Nest, The Andersons Lab Bedding, Maumee, OH, USA). Mice were fed autoclaved or irradiated Purina Lab Diet, product no. 5R31 (LabDiet, St. Louis, MO, USA).

AAV gene delivery

Viral vectors were delivered by retro-orbital systemic injection at a dose of 1×10^{11} GC/pup on DOL 0. All mice were housed with their mother and littermates and were handled by the same two researchers. Mice were compared to control littermates at 3 weeks post-treatment. Organ dissections were performed following euthanasia at day 21 of life under a dissecting microscope to remove the brain, heart, liver, skeletal muscle, and kidneys. Samples processed for immunohistochemistry and RNA *in situ* hybridization were immediately placed in freshly mixed 4% paraformaldehyde (PFA) fixative. Other organs were snap frozen prior to storage at −80°C and subsequent processing. Mice maintained for longevity studies were similarly treated by retro-orbital systemic injection at a dose

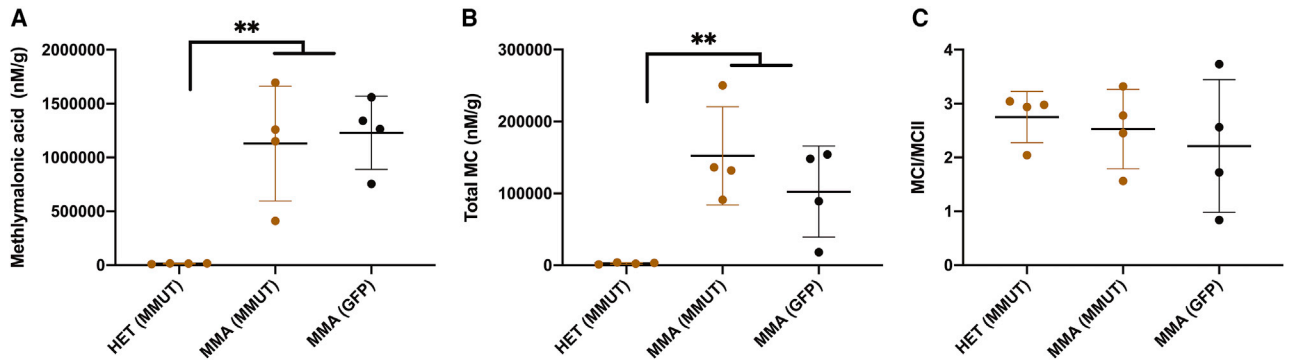

Figure 9. Effect of gene therapy on brain tissue metabolites

Methylmalonic acid and 2-methylcitrate (MC) measured in whole-brain tissue homogenate shown stratified by group in *Mmut*$^{+/-}$ (labeled HET) or *Mmut*$^{-/-}$;Tg$^{INS\text{-}MCK\text{-}Mmut}$ mice (labeled MMA), injected with a reporter (GFP, control vector) or treatment PHP.eB-CaMKII-MMUT vector (labeled MMUT). Metabolite levels were corrected for brain tissue wet weight. (A) Methylmalonic acid was significantly lower in HET mice that were treated with PHP.eB-CaMKII-MMUT (n = 4) compared to MMA mice regardless either treated with MMUT or with GFP reporter, but MMA mice did not (n = 4, p = 0.76). (B) Total MC was also significantly lower in HET mice ($p < 0.02$, n = 4 all groups) but not significantly different when comparing MMUT-treated to GFP-treated MMA mice (p = 0.42). (C) The ratio MCI/MCII was not significantly different across groups (ANOVA p = 0.69, n = 4 all groups).

of 1e11 GC/pup on DOL 0. Retro-orbital blood draws were obtained and body weights and metabolites were monitored monthly.

Metabolite studies

Plasma was isolated after retro-orbital collection of blood in tubes that contained 1–5 μL of diluted sodium heparin. The samples were immediately centrifuged, and the plasma was removed, diluted in water, and stored at −80°C in a screw-top tube for later analysis. Plasma samples were analyzed by gas chromatography-mass spectrometry with stable isotopic internal calibration to measure methylmalonic acid, 2-MC stereoisomer I (2S,3R and 2R,3S enantiomers), and 2-MC stereoisomer II (2S,3S and 2R,3R enantiomers) as described.[36] To measure brain parenchymal metabolite levels, whole-brain tissue was collected, wet weight was measured, and tissue was homogenized mechanically. Samples were then diluted in water and stored at −80°C in a screw-top tube for later analysis in the same manner as plasma samples described above.

Immunohistochemistry

Brain sections were evaluated for GFP fluorescence after counterstaining with DAPI (4′,6-diamidino-2-phenylindole) alone or DAPI with NeuN (hexaribonucleotide binding protein-3).[37–39] Slides were digitized with an Aperio ScanScope XT (Leica) at 200× in a single z plane, with lower magnifications shown as indicated. Fluorescence is quantified using visual assessment and image analysis by brain region, including the cerebrum, cerebellum, pons, hippocampus, thalamus, striatum, and choroid plexus. No GFP or NeuN signal was observed in negative control brain tissue. Fluorescence signal was quantified using a semiquantitative scoring method (visual) and using image analysis.[40] Image analysis is reported as number of cells meeting three separate fluorescence thresholds using a scale of 0–3+ as follows: 0: no staining, 1+: mild staining, 2+: moderate staining, 3+: strong staining. An H-score [1] was calculated using QuPath as follows: H-score = [1 × (% cells 1+) + 2 × (% cells 2+) + 3 × (% cells 3+)].[40,41]

RNA *in situ* hybridization

Tissue was fixed in 4% PFA, processed into paraffin blocks, and cut into 5-μm sections. Tissue sections were evaluated and quantified for the presence of RNA transcripts using chromogenic *in situ* hybridization probes for transgene (RNAscope target probe synMUT1 cat. no. 300031, Advanced Cell Diagnostics, Newark, CA, USA) or for native Mmut (cat. no. 322300, Advanced Cell Diagnostics, Newark, CA, USA) according to manufacturer's recommendations. Slides were digitized with an Aperio ScanScope XT (Leica) at 200× in a single z plane. Aperio whole-slide images were evaluated, and a threshold for positivity was determined using positive and negative controls. Cell detection algorithms were run to assess the positive cells. H-score was calculated using QuPath.[40,41] DAB staining is quantified using image analysis by tissue and by sub-anatomic region for the brain, including the cerebrum, cerebellum, pons, hippocampus, thalamus, striatum, and midbrain.

Vector genome quantitation

Brain and liver samples were collected at day 21 of life for both treated and control mice. Genomic DNA from tissue was extracted using DNeasy Blood & Tissue Kit (QIAGEN, Germantown, MD, USA; cat. no. 69506). ddPCR was performed according to the manufacturer's recommendations for the BioRad QX200 AutoDG ddPCR system using 10 ng or 20 ng of DNA as input and the following probes: Bio-Rad (Hercules, CA, USA) ddPCR CNV assay Gapdh (cat. no. 10042961, dMumCNS300520369) and MMUT (cat. no. 10042958, dCNS513322846).

Western blotting

Whole-tissue extracts from the mouse brain deep gray matter or liver were analyzed by immunoblotting and were probed with primary

rabbit polyclonal antibody against the methylmalonyl-CoA mutase enzyme (ab134956 Abcam, Cambridge, MA, USA), GFP (ab6556 Abcam, Cambridge, MA, USA), or β-actin (66009-1-Ig, Proteintech, Rosemont, IL, USA). The anti-MMUT antibody was used at a dilution of 1:1,000, and beta-actin was used at 1:10,000. Detection was performed with the Odyssey imaging system using the following secondary antibodies: IRDye 800CW donkey anti-rabbit IgG secondary antibody (LI-COR Biosciences) and IRDye 680RD donkey anti-mouse IgG (LI-COR Biosciences).

Statistical analysis

We calculated and reported the cohort average and standard error of the mean for methylmalonic acid, 2-methylcitrate, and RNAscope H-score. Figures show mean ± standard error of the mean unless otherwise indicated. Comparisons between two groups were performed using a non-parametric unpaired two-tailed t test, and comparisons among multiple groups were performed using a one-way ANOVA, with Tukey's multiple comparison post-test. A p value < 0.05 was considered significant. Homoscedasticity and normality assumptions were assessed. Statistical tests were performed using the software GraphPad Prism 8.3.0. Mouse studies were powered for the primary outcome, to identify a difference between serum methylmalonic acid levels in untreated $Mmut^{-/-}$;$Tg^{INS\text{-}MCK\text{-}Mmut}$ versus MMUT-treated mice when compared using a one-tailed t test. We used a conservative estimate of 2 for the effect size, meaning essentially that the difference in means between groups is expected to be more than 2 standard deviations, as seen in previous studies.[15] For a desired alpha of 0.05 and target power of >0.9, the predicted required sample size is 6 mice per group. Power analysis was performed using the Gpower program.

SUPPLEMENTAL INFORMATION

Supplemental information can be found online at https://doi.org/10.1016/j.omtm.2021.04.005.

ACKNOWLEDGMENTS

R.J.C., L.E.V., and C.P.V. were supported by the intramural research program of the NHGRI under 1Z01HG200318-15. P.E.H. was supported by an intramural research program PRAT postdoctoral fellowship. F.J.M. was supported by the NIH Medical Research Scholars Program, a public-private partnership supported jointly by the NIH and contributions to the Foundation for the NIH from the Doris Duke Charitable Foundation, Genentech, the American Association for Dental Research, the Colgate-Palmolive Company, and other private donors. We acknowledge the National Cancer Institute collaboration from the Pathology and Histology Laboratory for help with RNA in situ hybridization, and Darwin Romero for assistance with mouse studies.

AUTHOR CONTRIBUTIONS

F.J.M. prepared the manuscript and performed vector cloning, mouse experiments, western blot experiments, data analysis, and study design. R.J.C. prepared the manuscript and designed and supervised the studies. P.E.H. and L.E.V. assisted with experiments and edited the manuscript. C.P.V. designed and supervised the studies and edited the manuscript.

DECLARATION OF INTERESTS

The NIH has filed patents related to MMUT AAV gene therapy vectors on behalf of R.J.C. and C.P.V.

REFERENCES

1. Manoli, I., Sloan, J.L., and Venditti, C.P. (1993). Isolated Methylmalonic Acidemia. In In GeneReviews, M.P. Adam, H.H. Ardinger, R.A. Pagon, and S.E. Wallace, eds. (Seattle: University of Washington).
2. An, D., Schneller, J.L., Frassetto, A., Liang, S., Zhu, X., Park, J.S., Theisen, M., Hong, S.J., Zhou, J., Rajendran, R., et al. (2017). Systemic Messenger RNA Therapy as a Treatment for Methylmalonic Acidemia. Cell Rep. *21*, 3548–3558.
3. Carrillo-Carrasco, N., Chandler, R.J., Chandrasekaran, S., and Venditti, C.P. (2010). Liver-directed recombinant adeno-associated viral gene delivery rescues a lethal mouse model of methylmalonic acidemia and provides long-term phenotypic correction. Hum. Gene Ther. *21*, 1147–1154.
4. Chandler, R.J., and Venditti, C.P. (2016). Gene Therapy for Metabolic Diseases. Transl. Sci. Rare Dis. *1*, 73–89.
5. Chandler, R.J., and Venditti, C.P. (2019). Gene Therapy for Methylmalonic Acidemia: Past, Present, and Future. Hum. Gene Ther. *30*, 1236–1244.
6. Chakrapani, A., Sivakumar, P., McKiernan, P.J., and Leonard, J.V. (2002). Metabolic stroke in methylmalonic acidemia five years after liver transplantation. J. Pediatr. *140*, 261–263.
7. Yap, S., Vara, R., and Morais, A. (2020). Post-transplantation Outcomes in Patients with PA or MMA: A Review of the Literature. Adv. Ther. *37*, 1866–1896.
8. Baker, E.H., Sloan, J.L., Hauser, N.S., Gropman, A.L., Adams, D.R., Toro, C., Manoli, I., and Venditti, C.P. (2015). MRI characteristics of globus pallidus infarcts in isolated methylmalonic acidemia. AJNR Am. J. Neuroradiol. *36*, 194–201.
9. Thompson, G.N., Christodoulou, J., and Danks, D.M. (1989). Metabolic stroke in methylmalonic acidemia. J. Pediatr. *115*, 499–500.
10. Chandler, R.J., Williams, I.M., Gibson, A.L., Davidson, C.D., Incao, A.A., Hubbard, B.T., Porter, F.D., Pavan, W.J., and Venditti, C.P. (2017). Systemic AAV9 gene therapy improves the lifespan of mice with Niemann-Pick disease, type C1. Hum. Mol. Genet. *26*, 52–64.
11. Wang, D., Tai, P.W.L., and Gao, G. (2019). Adeno-associated virus vector as a platform for gene therapy delivery. Nat. Rev. Drug Discov. *18*, 358–378.
12. Manoli, I., Sysol, J.R., Epping, M.W., Li, L., Wang, C., Sloan, J.L., Pass, A., Gagné, J., Ktena, Y.P., Li, L., et al. (2018). FGF21 underlies a hormetic response to metabolic stress in methylmalonic acidemia. JCI Insight *3*, e124351.
13. Manoli, I., Sysol, J.R., Li, L., Houillier, P., Garone, C., Wang, C., Zerfas, P.M., Cusmano-Ozog, K., Young, S., Trivedi, N.S., et al. (2013). Targeting proximal tubule mitochondrial dysfunction attenuates the renal disease of methylmalonic acidemia. Proc. Natl. Acad. Sci. USA *110*, 13552–13557.
14. Manoli, I., Sysol, J., Li, L., Chandler, R., Senac, J., Hoffmann, V., Zerfas, P., Schnermann, J., and Venditti, C.P. (2011). Muscle targeted transgene expression rescues the lethal phenotype of Mut knockout mice. Mol. Genet. Metab. 102–248.
15. Chandler, R.J., Sloan, J., Fu, H., Tsai, M., Stabler, S., Allen, R., Kaestner, K.H., Kazazian, H.H., and Venditti, C.P. (2007). Metabolic phenotype of methylmalonic acidemia in mice and humans: the role of skeletal muscle. BMC Med. Genet. *8*, 64.
16. Wong, E.S., McIntyre, C., Peters, H.L., Ranieri, E., Anson, D.S., and Fletcher, J.M. (2014). Correction of methylmalonic aciduria in vivo using a codon-optimized lentiviral vector. Hum. Gene Ther. *25*, 529–538.
17. Ruppert, T., Schumann, A., Gröne, H.J., Okun, J.G., Kölker, S., Morath, M.A., and Sauer, S.W. (2015). Molecular and biochemical alterations in tubular epithelial cells of patients with isolated methylmalonic aciduria. Hum. Mol. Genet. *24*, 7049–7059.
18. Forny, P., Schumann, A., Mustedanagic, M., Mathis, D., Wulf, M.A., Nägele, N., Langhans, C.D., Zhakupova, A., Heeren, J., Scheja, L., et al. (2016). Novel Mouse Models of Methylmalonic Aciduria Recapitulate Phenotypic Traits with a Genetic Dosage Effect. J. Biol. Chem. *291*, 20563–20573.

19. Ballhausen, D., Mittaz, L., Boulat, O., Bonafé, L., and Braissant, O. (2009). Evidence for catabolic pathway of propionate metabolism in CNS: expression pattern of methylmalonyl-CoA mutase and propionyl-CoA carboxylase alpha-subunit in developing and adult rat brain. Neuroscience *164*, 578–587.

20. Mendell, J.R., Al-Zaidy, S., Shell, R., Arnold, W.D., Rodino-Klapac, L.R., Prior, T.W., Lowes, L., Alfano, L., Berry, K., Church, K., et al. (2017). Single-Dose Gene-Replacement Therapy for Spinal Muscular Atrophy. N. Engl. J. Med. *377*, 1713–1722.

21. Chan, K.Y., Jang, M.J., Yoo, B.B., Greenbaum, A., Ravi, N., Wu, W.L., Sánchez-Guardado, L., Lois, C., Mazmanian, S.K., Deverman, B.E., and Gradinaru, V. (2017). Engineered AAVs for efficient noninvasive gene delivery to the central and peripheral nervous systems. Nat. Neurosci. *20*, 1172–1179.

22. Ravindra Kumar, S., Miles, T.F., Chen, X., Brown, D., Dobreva, T., Huang, Q., Ding, X., Luo, Y., Einarsson, P.H., Greenbaum, A., et al. (2020). Multiplexed Cre-dependent selection yields systemic AAVs for targeting distinct brain cell types. Nat. Methods *17*, 541–550.

23. Gray, S.J., Foti, S.B., Schwartz, J.W., Bachaboina, L., Taylor-Blake, B., Coleman, J., Ehlers, M.D., Zylka, M.J., McCown, T.J., and Samulski, R.J. (2011). Optimizing promoters for recombinant adeno-associated virus-mediated gene expression in the peripheral and central nervous system using self-complementary vectors. Hum. Gene Ther. *22*, 1143–1153.

24. Jackson, K.L., Dayton, R.D., Deverman, B.E., and Klein, R.L. (2016). Better Targeting, Better Efficiency for Wide-Scale Neuronal Transduction with the Synapsin Promoter and AAV-PHP.B. Front. Mol. Neurosci. *9*, 116.

25. Hanlon, K.S., Meltzer, J.C., Buzhdygan, T., Cheng, M.J., Sena-Esteves, M., Bennett, R.E., Sullivan, T.P., Razmpour, R., Gong, Y., Ng, C., et al. (2019). Selection of an Efficient AAV Vector for Robust CNS Transgene Expression. Mol. Ther. Methods Clin. Dev. *15*, 320–332.

26. Wajner, M. (2019). Neurological manifestations of organic acidurias. Nat. Rev. Neurol. *15*, 253–271.

27. Allen, R.H., Stabler, S.P., Savage, D.G., and Lindenbaum, J. (1993). Elevation of 2-methylcitric acid I and II levels in serum, urine, and cerebrospinal fluid of patients with cobalamin deficiency. Metabolism *42*, 978–988.

28. Kölker, S., Sauer, S.W., Surtees, R.A., and Leonard, J.V. (2006). The aetiology of neurological complications of organic acidaemias–a role for the blood-brain barrier. J. Inherit. Metab. Dis. *29*, 701–704, discussion 705–706.

29. Sauer, S.W., Okun, J.G., Fricker, G., Mahringer, A., Müller, I., Crnic, L.R., Mühlhausen, C., Hoffmann, G.F., Hörster, F., Goodman, S.I., et al. (2006). Intracerebral accumulation of glutaric and 3-hydroxyglutaric acids secondary to limited flux across the blood-brain barrier constitute a biochemical risk factor for neurodegeneration in glutaryl-CoA dehydrogenase deficiency. J. Neurochem. *97*, 899–910.

30. Sauer, S.W., Opp, S., Mahringer, A., Kamiński, M.M., Thiel, C., Okun, J.G., Fricker, G., Morath, M.A., and Kölker, S. (2010). Glutaric aciduria type I and methylmalonic aciduria: simulation of cerebral import and export of accumulating neurotoxic dicarboxylic acids in in vitro models of the blood-brain barrier and the choroid plexus. Biochim. Biophys. Acta *1802*, 552–560.

31. Gao, B., and Meier, P.J. (2001). Organic anion transport across the choroid plexus. Microsc. Res. Tech. *52*, 60–64.

32. Hordeaux, J., Wang, Q., Katz, N., Buza, E.L., Bell, P., and Wilson, J.M. (2018). The Neurotropic Properties of AAV-PHP.B Are Limited to C57BL/6J Mice. Mol. Ther. *26*, 664–668.

33. Hordeaux, J., Yuan, Y., Clark, P.M., Wang, Q., Martino, R.A., Sims, J.J., Bell, P., Raymond, A., Stanford, W.L., and Wilson, J.M. (2019). The GPI-Linked Protein LY6A Drives AAV-PHP.B Transport across the Blood-Brain Barrier. Mol. Ther. *27*, 912–921.

34. Donsante, A., Yi, L., Zerfas, P.M., Brinster, L.R., Sullivan, P., Goldstein, D.S., Prohaska, J., Centeno, J.A., Rushing, E., and Kaler, S.G. (2011). ATP7A gene addition to the choroid plexus results in long-term rescue of the lethal copper transport defect in a Menkes disease mouse model. Mol. Ther. *19*, 2114–2123.

35. Lock, M., Alvira, M., Vandenberghe, L.H., Samanta, A., Toelen, J., Debyser, Z., and Wilson, J.M. (2010). Rapid, simple, and versatile manufacturing of recombinant adeno-associated viral vectors at scale. Hum. Gene Ther. *21*, 1259–1271.

36. Willard, H.F., Ambani, L.M., Hart, A.C., Mahoney, M.J., and Rosenberg, L.E. (1976). Rapid prenatal and postnatal detection of inborn errors of propionate, methylmalonate, and cobalamin metabolism: a sensitive assay using cultured cells. Hum. Genet. *34*, 277–283.

37. Misteli, T., and Spector, D.L. (1997). Applications of the green fluorescent protein in cell biology and biotechnology. Nat. Biotechnol. *15*, 961–964.

38. Lavezzi, A.M., Corna, M.F., and Matturri, L. (2013). Neuronal nuclear antigen (NeuN): a useful marker of neuronal immaturity in sudden unexplained perinatal death. J. Neurol. Sci. *329*, 45–50.

39. Kapuscinski, J. (1995). DAPI: a DNA-specific fluorescent probe. Biotech. Histochem. *70*, 220–233.

40. Bankhead, P., Loughrey, M.B., Fernández, J.A., Dombrowski, Y., McArt, D.G., Dunne, P.D., McQuaid, S., Gray, R.T., Murray, L.J., Coleman, H.G., et al. (2017). QuPath: Open source software for digital pathology image analysis. Sci. Rep. *7*, 16878.

41. McCarty, K.S., Jr., Miller, L.S., Cox, E.B., Konrath, J., and McCarty, K.S., Sr. (1985). Estrogen receptor analyses. Correlation of biochemical and immunohistochemical methods using monoclonal antireceptor antibodies. Arch. Pathol. Lab. Med. *109*, 716–721.